International Journal of Solids and Structures 45 (2008) 5059–5073

Contents lists available at ScienceDirect

International Journal of Solids and Structures

journal homepage: www.elsevier.com/locate/ijsolstr

Discrete modeling of crack bridging by a discontinuous platelet with a controlled interface

Scott E. Sanborn *, Jean H. Prévost

Department of Civil and Environmental Engineering, Princeton University, Princeton, NJ 08544, USA

ARTICLE INFO

Article history:
Received 3 July 2007
Received in revised form 27 March 2008
Available online 24 May 2008

Keywords:
Fiber-matrix interface
Crack bridging
Fiber pullout
Stress concentrations
Finite element

ABSTRACT

Crack bridging by discontinuous fibers can make brittle materials tougher by transferring stresses from the crack tip to elsewhere in the matrix material. One important aspect of crack bridging is the nature of the interface between the fibers and the matrix material. In this paper, a two-dimensional numerical model of bridging a Mode I loaded crack by linear elastic discontinuous platelets is developed for two different types of interfaces. The first type is a perfectly bonded interface. The second type is an imperfect interface described as a stick–slip interface. A shear-lag model to predict platelet pullout is developed in detail to verify the numerical implementation of the stick–slip interface. An example of a crack tip bridged by a platelet is examined for both interfaces. The perfectly bonded interface will reduce the Stress Intensity Factor (SIF) of the crack greatly but introduces new stress concentrations at the platelet ends. The stick–slip interface can be tailored to also reduce the SIF while not introducing new stress concentrations.

1. Introduction

Many brittle materials are made tougher by adding second phase materials such as discontinuous fibers. This added toughness is the result of crack bridging by these second phase materials. Crack bridging reduces the Stress Intensity Factor (SIF) of the crack and transfers stresses elsewhere in the material. It is this transfer of stress that results in the formation of many small width cracks rather than one large width crack. This process of distributing deformation throughout the composite is vital for toughening brittle materials.

One important class of composites that have achieved success in making brittle materials tougher with discontinuous fibers is Engineered Cementitious Composites (ECCs). By taking a micromechanical approach to composite design, ECCs have been shown to develop distributed deformation under tensile loading (Li, 2003; Li, 1993). It has been shown that the complementary energy of the bridged cracks is an important indicator as to whether or not distributed deformation will occur (Li and Wu, 1992; Marshall and Cox, 1988). This complementary energy is based on a crack bridging law of the composite, which is in turn based on the properties of the fiber, the matrix, and the interface.

While complementary energy is an important indicator for distributed deformation it does provide knowledge of the stress distributions near the embedded ends of the fibers. This is highly dependent on the interface. Much attention, in the form of experimental studies, has been paid to modifying the interface properties between the matrix and the fiber reinforcement (Redon et al., 2001; Kanda and Li, 1998). However, there is a lack of understanding of the effect the interface has on the stresses in the matrix material, particularly at the ends of the fibers.

* Corresponding author. Tel.: +1 609 258 8439.
E-mail address: ssanborn@princeton.edu (S.E. Sanborn).

0020-7683/$ - see front matter © 2008 Elsevier Ltd. All rights reserved.
doi:10.1016/j.ijsolstr.2008.05.008

This paper will examine the role of the interface through the discrete modeling of platelets in a matrix. In this paper through thickness platelets bridging a two-dimensional crack are studied since fibers cannot easily be represented in a planar geometry. Though there exist crack bridging models that approximate the bridging by individual fibers as a continuous closing traction applied to the crack surface, such as in Marshall and Cox (1988), we will explore a discrete numerical model of crack bridging to observe what happens to the stresses in the surrounding matrix. A comparison of discrete and continuous models for crack-bridging (Carpinteri and Massabó, 1997) has shown both models produce similar macroscopic behaviors. Discrete modeling of random fibers reinforcing a brittle matrix has been achieved with lattice models that use Voronoi tessellation for the matrix and Delaunay tessellation for a spring or beam network (Bolander and Saito, 1997; Bolander and Saito, 1998; Bolander and Sukumar, 2005). This paper will develop a model similar to those Voronoi cell models but based in a standard Finite Element (FE) framework. Also, a method of explicitly representing the interface between the platelet and the matrix is developed.

This paper first describes the two different types of interfaces to be used; a perfectly bonded interface and a stick–slip interface. An analytical shear-lag model is developed to describe the pullout of a platelet with the stick–slip interface. Next the implementation of both interfaces into a FE model is described and the numerical stick–slip pullout is checked against the analytical model. Both interfaces are then implemented into a FE model for bridging of a Mode I crack.

Finally, results from the two different interfaces are compared. The most important result found is that the perfectly bonded interface introduces new stress concentrations at the ends of the platelets under certain conditions. The matrix may fail at these stress concentrations leading to a composite having a lower toughness than predicted. This phenomenon has been observed experimentally (Kanda and Li, 2006). It is referred to as plug pullout phenomenon, shown in Fig. 1. Plug pullout phenomenon occurs when groups of fibers act together to pullout a portion of the matrix separated from the rest of the matrix near the ends of the fibers. The stick–slip interface is found to avoid the creation of these extra stress concentrations while still significantly reducing the SIF of the main crack.

2. Description of perfectly bonded and stick–slip interfaces

The first type of interface considered is the perfectly bonded interface. A perfectly bonded interface requires that the deformations in the matrix and fiber be equal at the interface along the length of the fiber. This assumption is applicable to a composite system in which the matrix cracks under much lower stresses than any occurrence of interface failure. In other words, relative to the matrix, the interface is very strong.

The second type of interface that will be considered in this paper is the stick–slip interface. The stick–slip interface will be based on a one-dimensional shear-lag model with a simple assumed relationship between the local slip, $S(x)$, and the local shear stress $\tau(x)$ at any point x along the interface. The local slip is defined as the difference between the platelet displacement, δ_p, and the matrix displacement, δ_m, at a point x along the interface.

$$S(x) = \delta_p(x) - \delta_m(x) \tag{1}$$

In shear-lag models all of the stress is assumed to be transferred from the fiber to the matrix through a very thin interface layer that can only carry shear stress. This model is applicable if the strains normal to the fiber are much smaller than the strains parallel to the fiber. Therefore, the displacements in Eq. 1 are only defined parallel to the fiber. Many models exist describing the force-displacement or stress-slip relationship for the pullout of fibers (Carpinteri et al., 2006; Leung and Li, 1991; Naaman et al., 1991A). Fig. 2 shows the assumed relationship between $S(x)$ and $\tau(x)$ for any point x on the interface

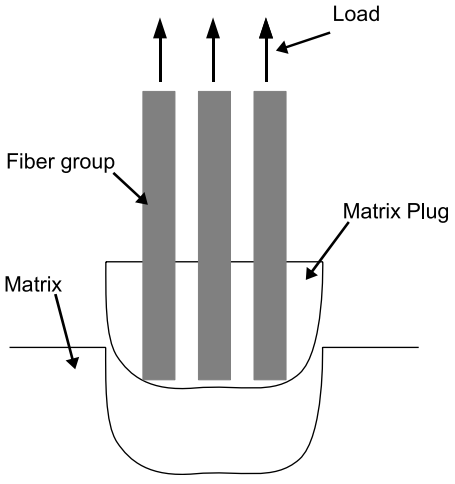

Fig. 1. Schematic of plug pullout.

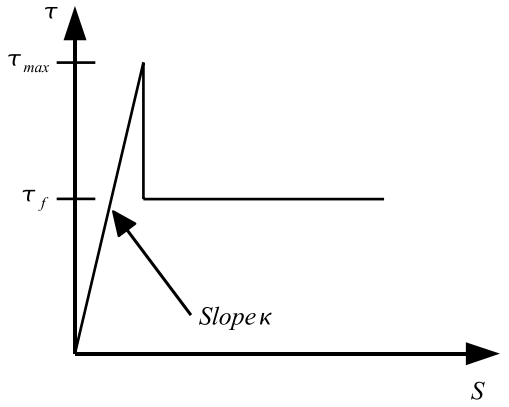

Fig. 2. Assumed relationship between local shear stress and local slip.

chosen for this study. Initially the interface is in the "stick" regime, where the shear stress is linearly related to the slip by the bond modulus κ. The interface can carry a maximum shear stress, τ_{max}, at which the bond between the fiber and matrix fails. Upon further slip the interface enters the "slip" regime which is controlled by the frictional shear stress τ_f. It is understood that the use of a constant frictional shear stress greatly simplifies the real slip behavior. Since the strains perpendicular to the fiber are ignored any changes on the frictional stress due to deformations in the perpendicular direction are ignored. The use of a constant frictional shear stress also ignores any change in frictional shear stress due to degradation of the fiber, matrix, or interface that may occur during slip. Thus the assumed relationship between $S(x)$ and $\tau(x)$ depends the three parameters: κ, τ_{max}, and τ_f. This assumed relationship was previously introduced in the work of Naaman et al. (1991A). In the limiting case that κ and τ_{max} approach infinity the perfectly bonded interface is recovered. It should be noted that in both the interfaces described above no failure of the fiber, such as fiber rupture or yielding, is considered.

3. Derivation of stick–slip pullout equations

Pullout equations will be developed for the stick–slip interface. These will be used to validate the numerical stick–slip interface presented later. Similar shear-lag models have been used to develop pullout equations of a fiber from a matrix (Naaman et al., 1991A; Leung and Li, 1991). In Naaman et al. (1991A), there is an error in the pullout equations and only one way slip regime formation is considered. In Leung and Li (1991), two way slip regime formation is considered but the interface is essentially considered perfect until τ_{max} is reached.

First the geometry of the pullout specimen, as shown in Fig. 3, will be described. The specimen consists of a matrix material of cross-sectional area A_m and width w. Embedded in this matrix material is a platelet of initial length l, width w, and thickness t, such that it has cross-sectional area $A_p = wt$. The perimeter per unit length of the platelet is, $\psi = 2w$. Prior to loading, the free end of the platelet is aligned with the free end of the matrix. Distance along the platelet is measured from the embedded end along the x axis as shown in Fig. 4. Under an applied load, P, the free end of the platelet will be displaced relative to the matrix by an amount Δ_l. The embedded end of the platelet is assumed to have negligible end anchorage.

Using the assumed stick–slip relationship between $\tau(x)$ and $S(x)$, a similar procedure as used in Naaman et al. (1991A) is followed. We begin by taking a force balance on an infinitesimal segment of the platelet, leading to:

$$dF = \tau\psi dx \tag{2}$$

where F is the force in the platelet. Eq. (2) can be rearranged to form:

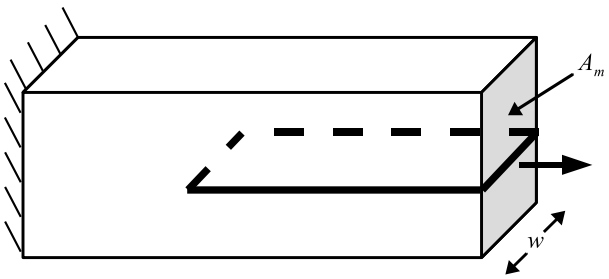

Fig. 3. Geometry of pullout specimen.

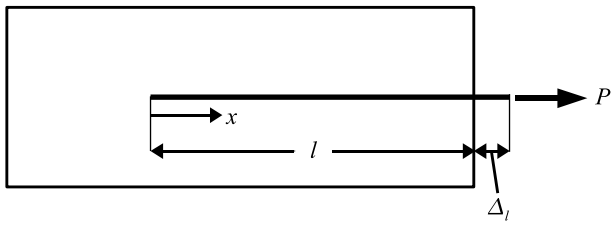

Fig. 4. Two-dimensional geometry of pullout specimen.

$$\frac{dF(x)}{dx} = \tau(x)\psi \tag{3}$$

Eq. (3) holds along the entire length of the platelet; for both stick and slip zones.

Next, we define the following dimensionless parameters:

$$Q = 1 + \frac{A_m E_m}{A_p E_p} \tag{4}$$

$$K = \frac{\psi\kappa}{A_m E_m} \tag{5}$$

$$\lambda = \sqrt{KQ} \tag{6}$$

where E_p and E_m are the Young's moduli of the platelet and the matrix respectively.

Differentiation of Eq. (3) along with static equilibrium and use of the dimensionless parameters just defined leads the following ordinary differential equation:

$$\frac{d^2F}{dx^2} - \lambda^2 F = -KP \tag{7}$$

Eq. (7) holds only for the stick zone of the platelet. Eq. (7) can be solved by a function of the following form:

$$F(x) = P(A_0 \cosh \lambda x + B_0 \sinh \lambda x + 1/Q) \tag{8}$$

Taking the derivative of $F(x)$ using the relation in Eq. (3), the shear distribution along the interface is:

$$\frac{dF}{dx}\frac{1}{\psi} = \tau(x) = \frac{P\lambda}{\psi}(A_0 \sinh \lambda x + B_0 \cosh \lambda x) \tag{9}$$

3.1. Full stick pullout

For the case of a fully stuck plate, meaning the entire interface is within the stick regime, the force in the platelet should be zero at the embedded end and P at the free end. Using these boundary conditions, the coefficients A_0 and B_0 in Eq. (8) become:

$$A_0 = -\frac{1}{Q}$$
$$B_0 = \frac{1+\frac{1}{Q}(\cosh \lambda l - 1)}{\sinh \lambda l} \tag{10}$$

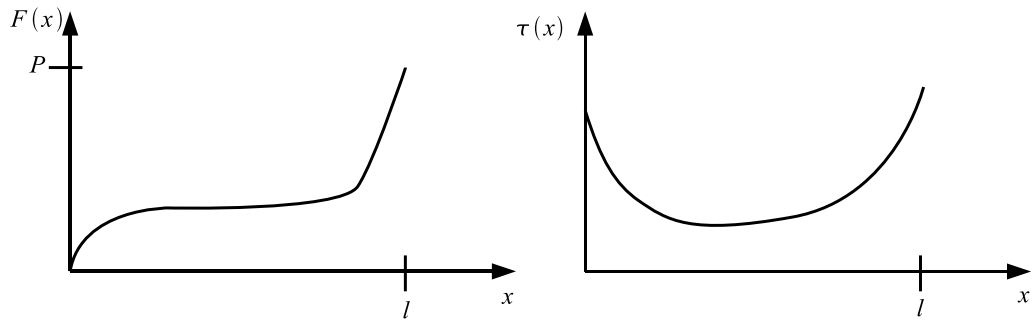

Fig. 5. Schematic of force and shear stress distributions for fully stuck platelet.

Typical distributions of the force in the platelet as well as the shear stress in the interface are shown in Fig. 5.

The slip in the interface can be found using the assumed relationship between $S(x)$and $\tau(x)$ shown in Fig. 2. Since the entire platelet is within the stuck regime Eq. (9) is used for $\tau\ (x)$. The slip at the free end of the platelet Δ_l is:

$$\Delta_l = S(l) = \frac{1}{\psi\kappa}\frac{\mathrm{d}F}{\mathrm{d}x}\bigg|_{x=l} \tag{11}$$

Since the platelet is fully stuck, it is restricted along its entire length and not free to elongate elastically. In Eq. (11) only the slip at the interface contributes to the slip at the free end. Upon subbing in the values for A_0 and B_0, Eq. (11) simplifies to:

$$\Delta_l = \frac{P\lambda}{Q\psi\kappa}\left(\frac{1+(Q-1)\cosh\lambda l}{\sinh\lambda l}\right) \tag{12}$$

As seen in Eq. (12) the end slip of the platelet, Δ_l, is a linear function of the applied load P for a fully stuck platelet.

The shear stress distribution,$\tau(x)$, determined from Eq. (9) gives local maxima at the free and embedded ends of the platelet. By comparing the shear stress at $x = 0$ and $x = l$, the end that reaches $\tau_{\max}$ first can be determined. This is the end where the slip regime is initiated. After some manipulation it can be shown that if the following is true:

$$Q < 2 \tag{13}$$

then $\tau_{\max}$ will be reached at the embedded end of the platelet first. A slip zone will initiate from the embedded end of the platelet. The loading at which it will initiate, P_{crit} is:

$$P_{\text{crit}} = \frac{\tau_{\max}\psi}{\lambda}\frac{1}{B_0} \tag{14}$$

Otherwise if:

$$Q > 2 \tag{15}$$

then the slip zone will initiate at the free end of the platelet and the loading at which it will initiate is:

$$P_{\text{crit}} = \frac{\tau_{\max}\psi}{\lambda}\left(\frac{1}{A_0\sinh\lambda l + B_0\cosh\lambda l}\right) \tag{16}$$

For the case of $Q = 2$, the slip zone will initiate simultaneously from both ends of the platelet and both expressions for P_{crit} will be equal.

3.2. Slip zone formation from free end, $Q > 2$

If Eq. (15) is true then once P_{crit} is reached the slip regime will form from the free end of the platelet. Eq. (7) still holds for the portion of the platelet that is still stuck while Eq. (3) holds for the entire platelet. The length of the slip zone of the platelet is denoted as l_1. The force in the platelet can be represented by the following two equations:

$$F_b(x) = P(A_1\cosh\lambda x + B_1\sinh\lambda x + 1/Q) \quad \text{for } 0 \leqslant x \leqslant l - l_1 \tag{17}$$

$$F_{f_1}(x) = \tau_f\psi(x-l) + P \quad \text{for } l - l_1 < x \leqslant l \tag{18}$$

Eq. (17) is the force for the stuck zone of the platelet while Eq. (18) is the force in the slip zone. Since the shear stress in the slip zone is constant Eq. (3) indicates that the force in the slip zone should be linear. Typical distributions of the force and shear stress along the platelet are shown in Fig 6. In order to create the pullout curve, values of l_1 between *0* and l must be incrementally chosen. For each value of l_1 the coefficients A_1 and B_1, as well as the loading value P, can be solved by applying

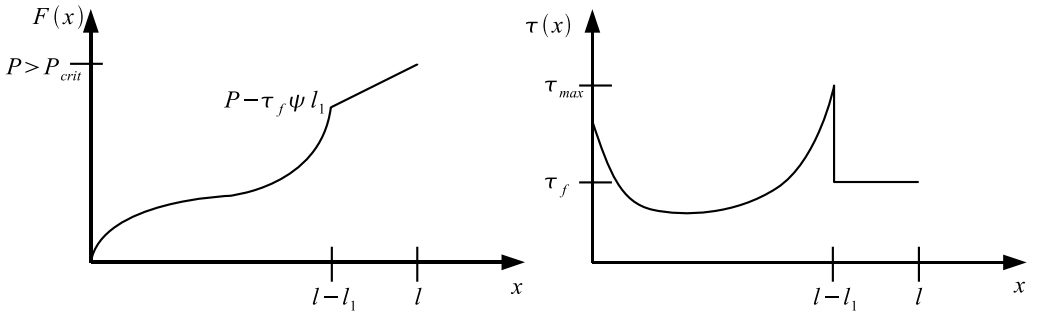

Fig. 6. Schematic of force and shear distributions for slip zone formation from free end.

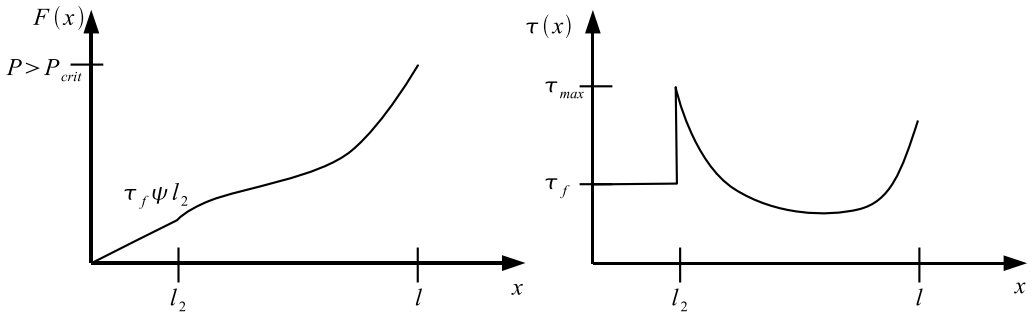

Fig. 7. Schematic of force and shear distributions for slip zone formation from embedded end.

the boundary conditions shown in Fig. 6. Upon solving for A_1, B_1 and P, the pullout of the platelet at the free end can be found as the sum of two terms. The first term is the slip at the end of the stick zone, the second term is the change in slip along the slip zone[1]. The change in slip accumulated along any portion a to b of the interface is defined as:

$$S_{ab} = \delta_p(b) - \delta_p(a) - \{\delta_m(b) - \delta_m(a)\} = \int_a^b \{\varepsilon_p(x) - \varepsilon_m(x)\}\mathrm{d}x \tag{19}$$

where $\varepsilon_p(x)$ and $\varepsilon_m(x)$ are the local strains in the platelet and matrix, respectively. Eq. (19) can be simplified to:

$$S_{ab} = \int_a^b \frac{Q}{A_m E_m} F(x)\mathrm{d}x - \frac{P(b-a)}{A_m E_m} \tag{20}$$

Therefore the total pullout at the free end of the platelet is:

$$\Delta_l = \frac{1}{\psi\kappa}\left.\frac{\mathrm{d}F_b}{\mathrm{d}x}\right|_{x=l-l_1} + \int_{l-l_1}^{l} \frac{Q}{A_m E_m} F_{f_1}(x)\mathrm{d}x - \frac{Pl_1}{A_m E_m} \tag{20}$$

Each value of l_1 will produce a unique value of P and Δ_l. For each value of l_1 the shear stress at the embedded end must be check to see if is still below $\tau_{\max}$. If it is not then two way slip zone formation will initiate.

3.3. Slip zone formation from embedded end, $Q < 2$

If Eq. (13) is true then a slip zone will initiate from the embedded end of the platelet once P_{crit} has been reached. Again Eq. (7) still holds for the stuck portion of the platelet while Eq. (3) holds for the entire plate. Let the slip zone length from the embedded end of the platelet be l_2 then the force in the platelet can be determined from the following:

$$F_b(x) = P(A_2 \cosh \lambda x + B_2 \sinh \lambda x + 1/Q) \quad \text{for } l_2 \leqslant x \leqslant l \tag{21}$$

$$F_{f_2}(x) = \tau_f \psi x \quad \text{for } 0 \leqslant x < l_2 \tag{22}$$

Eq. (21) represents the force in the stick zone while Eq. (22) represents the force in the slip zone at the embedded end of the platelet. Typical force and shear distributions for slip zone formation from the embedded end are shown in Fig. 7. Values of l_2 must be chosen incrementally. Applying the boundary conditions shown in Fig. 7 the values of the coefficients A_2,B_2 and the value of the load P can be solved for. Upon solving for A_2, B_2, and P, Eq. (3) may be used to solve for the pullout of the plate at the free end.

$$\Delta_l = \frac{1}{\psi\kappa}\left.\frac{\mathrm{d}F_b}{\mathrm{d}x}\right|_{x=l} \tag{23}$$

Each value of l_2 will produce a unique P and Δ_l. The shear stress at the free end of the plate must be checked for each l_2 to make sure it is below $\tau_{\max}$. If it is not then two way slip zone formation will initiate.

3.4. Two way slip zone formation

As the length of the slip zone (l_1 or l_2) increases the shear stress at the stick end may reach $\tau_{\max}$. If this is the case, or if $Q = 2$, then two way slip zone formation will initiate. If two way slip zone formation occurs, again Eq. (3) holds for the entire platelet while Eq. (7) only holds for the portion of the plate that is still stuck. The force in the slip zone of the embedded end is given by Eq. (22), and in the slip zone at the free end is given by Eq. (18). Typical force and shear distributions are shown in

[1] In Naaman et al. (1991A) expressions for Δ_l effectively neglect to include the instantaneous slip at the embedded end of the platelet. It is necessary to consider this instantaneous slip at the embedded end because this shear-lag model neglects any embedded end anchorage.

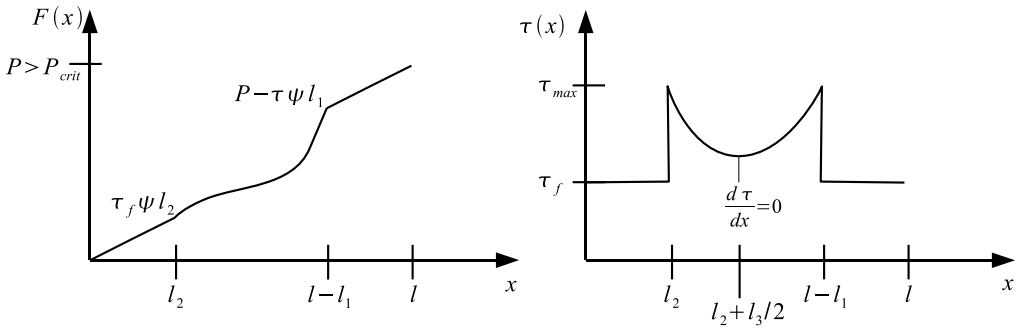

Fig. 8. Schematic of force and shear distributions for two way slip zone formation.

Fig. 8. Defining $l_3 = l\text{-}l_1\text{-}l_2$, the boundary conditions shown in Fig. 8 are applied.Using a procedure similar to one found in Leung and Li (1991) the total slip zone length $l_d = l_1 + l_2$ is chosen. Then P, l_1, $F(x)$ can be determined as:

$$P = \tau_f \psi (l_1 + l_2) - \frac{2\tau_m \psi}{\lambda}\left(\frac{1 - e^{\lambda l_3}}{1 + e^{\lambda l_3}}\right) \tag{24}$$

$$l_1 = \frac{1}{\psi \tau_f}\left[P\left(1 - \frac{1}{Q}\right) + \frac{\tau_m \psi}{\lambda}\left(\frac{1 - e^{\lambda l_3}}{1 + e^{\lambda l_3}}\right)\right] \tag{25}$$

$$F_b(x) = P - \tau_f \psi l_1 + \frac{\tau_m \psi}{\lambda}\frac{1}{1 + e^{\lambda l_3}}(1 - e^{-\lambda(x-(l-l_1))} + e^{-\lambda(l_2 - x)} - e^{\lambda l_3}) \tag{26}$$

Once these values are determined Eq. 20 can be used again to determine the end slip. The value of l_d is incrementally increased until the entire interface is in the slip regime. In Eqs. (20) and (23) only interface slip contributes to the free end slip. For cases where there is a slip zone at the free end, Eq. (20), it is possible that the free end of the platelet may experience some elastic elongation. In these equations Δ_l is assumed to be small enough such that elastic elongation in this portion of the platelet can be neglected.

3.5. Full slip pullout

Once the slip zone has formed along the full length of the platelet dynamic slip of the platelet will occur. Denoting the end slip accumulated until the onset of dynamic slip of the platelet as Δ_0 and any further dynamic slip of the platelet as u, as shown in Fig. 9, the free end force on the platelet can be determined as:

$$P = \tau_f \psi (l - u) \tag{27}$$

As noted in Kullaa (1998), the total slip at the end of the platelet can be written as the sum of the slip prior to dynamic slip, a dynamic slip term, and an elastic elongation of portion of the platelet that is outside of the matrix. The slip at the free end of the platelet becomes:

$$\Delta_l = \Delta_0 + u + \frac{Pu}{A_p E_p} \tag{28}$$

As stated earlier, this formulation assumes Δ_0 is small and neglects any elastic elongation in that portion. It should be noted that Eqs. (27) and (28) describe linear slip, where τ_f remains constant. Experimental evidence in fiber pullout tests (Redon et al., 2001; Naaman et al., 1991B) show that τ_f changes as the fiber pulls out. This is a result of slip softening or slip hardening, mechanisms which can greatly increase or decrease the work done during fiber pullout. The model developed here does not account for any of these mechanisms. Additionally, one dimensional shear-lag debonding theory neglects Pois-

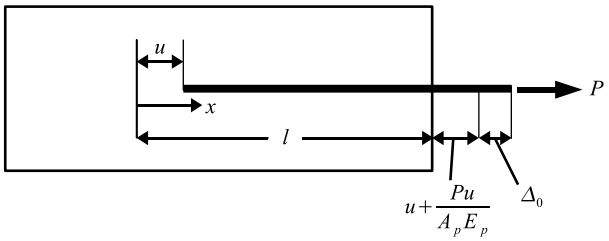

Fig. 9. Notation for slipping platelet.

son's effect on the platelet. As the platelet is subject to tension the thickness of the platelet will shrink, assuming a positive Poisson's ratio. In this case it is expected that the frictional stress would not be a constant since τ_f would vary depending on the load. Finally, the expressions developed in this paper for pullout load and displacement will not hold if at anytime during the pullout load is greater than the yielding load for the platelet.

All the necessary expressions for computing the pullout curve of a platelet embedded in a matrix of a given geometry and interface described by κ, $\tau_{\max}$, and τ_f have now been derived. A typical computed pullout curve is shown in Fig. 10. The pullout curves must be computed numerically as values of l_1, l_2, l_3, and u must be incrementally increased to determine P and Δ_l for each of those values. A pullout curve based on these expressions will be used to validate the finite element model of the stick–slip interface.

4. Finite element modeling of discrete crack bridging

In this paper, a two dimensional problem is considered. A slender specimen with a center crack in tension is considered as shown in Fig. 11. For this geometry the crack is in pure Mode I loading. The matrix material is assumed to be brittle and the yielding zone at the crack tip is assumed to be very small compared to the length of the crack; therefore Linear Elastic Fracture Mechanics (LEFM) assumptions apply. All length scales in this paper will be defined in terms of the half crack length a. For the specimen shown in Fig. 11, the half width of the specimen is $\frac{40}{11}a$ and the half height is $\frac{120}{11}a$. An empirical solution for the SIF of this test specimen is known and can be found in Tada et al. (2000). In the numerical model only the right half of this specimen is modeled. Symmetry boundary conditions are placed along the vertical center line shown in Fig. 11. The matrix material is modeled with standard four-noded quad elements in plane strain. The crack is modeled using the eXtended Finite Element Method (XFEM). In this method elements which are intersected by the crack are enriched with the Heaviside function and the elements near the crack tip are enriched with the crack tip functions which can exactly reproduce the displacement fields for a linear elastic crack tip. The details of this method are given in Prevost and Sukumar (2003).

The far field loading, σ_{far}, is incrementally increased in a displacement controlled loading method. The SIF is calculated using a domain integral method (Belytschko and Black, 1999). The radius of the domain integral used is 1.5 times the element height. This radius must be small enough to ensure that any platelets used to bridge the crack do not intersect the domain of the domain integral. Since the unbrided system is linear, the SIF is linearly proportional to σ_{far} and the SIF need only be checked under one arbitrary load. The SIF is found to be within 2.5% error compared to the asymptotic approximation by Koiter found in Tada et al. (2000). The unbridged SIF, K_{I0}, is used later to compare the improvements of bridging the crack with both the perfectly bonded interface as well as the stick–slip interface.

4.1. Finite element implementation of perfectly bonded interface

The specimen geometry described in the previous section is modeled with a platelet bridging the crack. The platelet of length $\frac{18}{11}a$ is placed a distance of $\frac{5}{11}a$ behind the crack tip. Because symmetry conditions are imposed the total crack is actually bridged by two platelets. The mesh near the crack tip is shown in Fig. 12. If the platelet is very thin it may be modeled by standard truss elements. Thicker platelets in which bending stiffness becomes important may be modeled by beam elements. In this paper, all platelets are considered to have negligible bending stiffness and are modeled with truss elements. The platelet is composed of several truss elements. Each truss spans the length of one continuum element. Its nodes and degrees of freedom are the same as those of the continuum elements. In this way, the platelets are perfectly bonded to the matrix material.

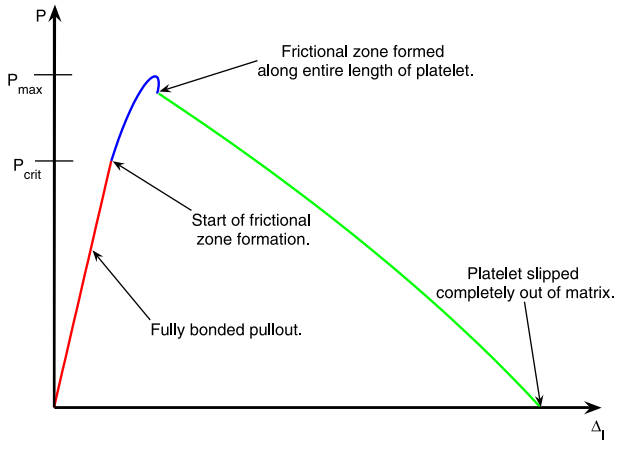

Fig. 10. Typical pullout curve.

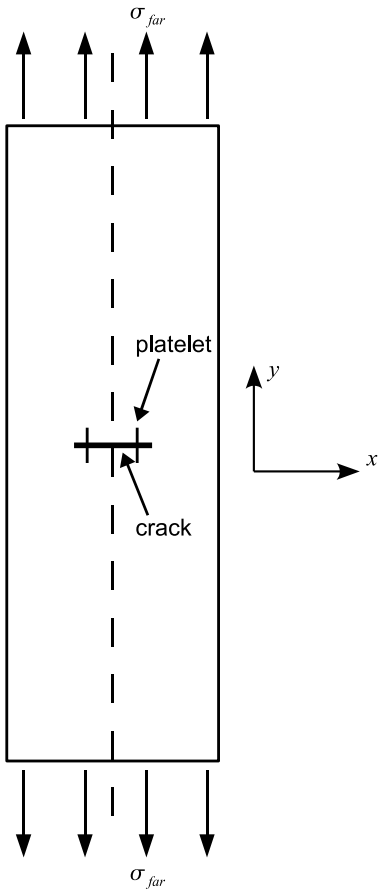

Fig. 11. Geometry of crack bridging model.

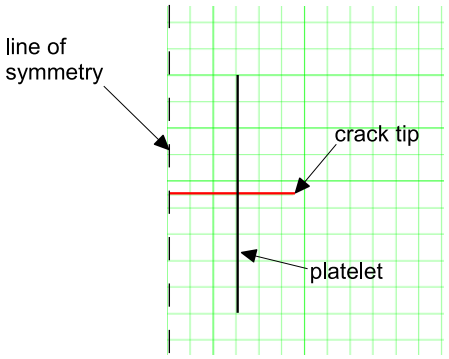

Fig. 12. Mesh near crack tip.

From the geometry of the problem an approximation of Q can be made, even though Q is a parameter defined for the single platelet pullout problem. As stated earlier, the perfectly bonded case is equal to the stick–slip interface if κ and $\tau_{\max}$ approach infinity. For the perfectly bonded case Q can indicate where the highest stresses will be observed along the platelet, at the embedded end or free end. A_m per unit thickness for both cases can be estimated as the area of one face of the crack half width, a, while A_p per unit thickness was set to approximately $0.02a^2$ giving $\frac{A_m}{A_p} \approx 50$. Two perfectly bonded composite systems were modeled. In the first system $\frac{E_m}{E_p} = 0.01$ giving $Q \approx 1.5$. This ratio of Young's moduli is in a range similar to exfoliated polymer/clay composites (Sheng et al., 2004). In the second system $\frac{E_m}{E_p} = 0.5$ giving $Q \approx 26$. This ratio of Young's moduli is similar to those of fibers used in ECCs (Kanda and Li, 2006).

Since the perfectly bonded systems are still linear, the SIF is still proportional to σ_{far} and need only be measured at one load step. Since the perfectly bonded systems are linear, the stress fields only change in magnitude from one load step to the

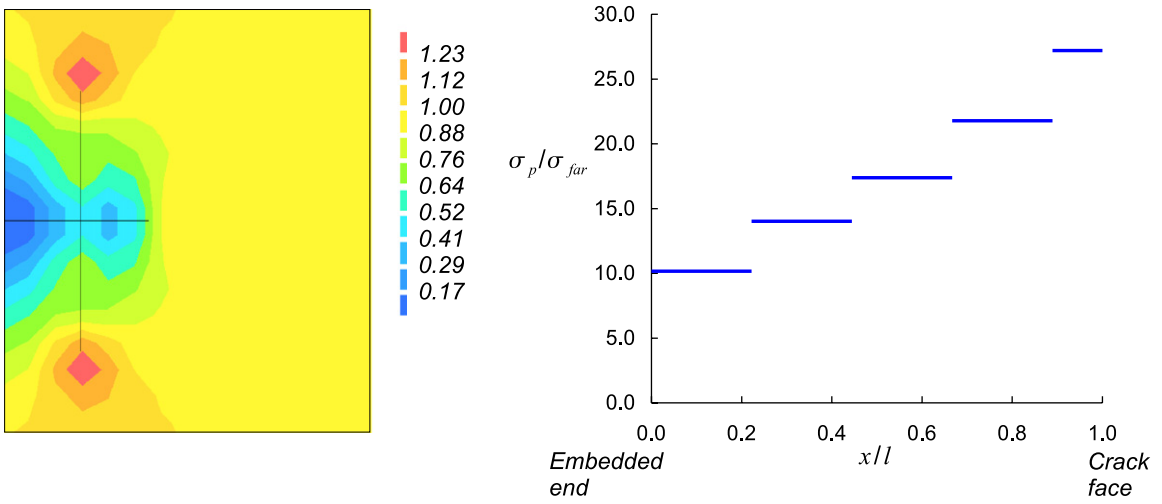

Fig. 13. Maximum principal stress distribution for platelet bridging a crack tip with a perfectly bonded interface, $Q \approx 1.5$. Note the stress concentrations at the ends of the platelets (left). Stress in each segment of one half of the platelet (right).

next. Fig. 13 gives the largest principal stress contours for the first system, $Q \approx 1.5$ along with the stress distribution for one half of the platelet, σ_p. As expected the highest principal stress is observed at the embedded ends of the platelet. These stresses are higher than those at the crack tip. For this system the high stresses at the embedded ends may be of concern. These stress concentrations could lead to fracture and plug pullout. This situation is exacerbated as the volume fraction of platelets is increased. Consider a case of the same composite system but with an added platelet for each crack tip. This reduces $\frac{A_m}{A_p} \approx 25$ leading to $Q \approx 1.25$. The largest principal stress contours for this case can be seen from Fig. 14. In this case, the stress concentrations are no longer isolated; instead a large swath of high stresses forms near the embedded ends of the platelets.

Fig. 15 gives the principal stress contours along with the stress distribution for one half of the platelet for the second system, $Q \approx 26$. In this system the highest stresses are observed at the crack tip, meaning for the case where $Q > 2$ plug pullout is not expected.

This overlaying truss representation of the platelet will only be valid when the volume fraction of the platelets is small and the aspect ratio, length to thickness, of the platelet is large. If the volume of the platelets is significant compared to that of the matrix there will be an excess of matrix material as it is not removed in place of the platelet. A proper way to model this in higher volume fractions would be to use continuum elements for the platelets. This model is also limited to pure Mode I loading as it does not appropriately account for mechanisms other than interface debonding and frictional sliding. In this paper we limit our studies to very thin platelets.

4.2. Finite element implementation of stick–slip interface

The implementation of this stick–slip interface into a FE framework will now be discussed. Similar to the case of the perfectly bonded interface, the platelets will be modeled by linear truss elements and the matrix by linear elastic four noded quads in plane strain. Unlike the perfectly bonded case, the truss elements are connected to the quad nodes via nodal links. A nodal link is a finite element that connects two nodes by a prescribed force-displacement relationship. The force-displacement relationship of the nodal links on the interior of the platelet for the stick–slip interface is shown in Fig. 16. As shown in Fig. 16, after some slip distance the force in the link must become zero. For end nodes all values of Δx in Fig. 16 would be replaced by $\Delta x/2$. These nodal links discretize the shear stress versus slip relationship shown in Fig. 2. This force-displacement relationship only applies to displacements along the axis of the platelet. Any displacements perpendicular to the axis of the platelets are exactly the same as the corresponding matrix nodes. Since the force in the nodal links is described by a multi-linear function of the displacement, the displacements of the quads and trusses must now be solved by an iterative scheme. At test problem for pullout of a platelet attached to a matrix with a stick–slip interface was implemented. The resulting pullout curve was found to converge to the analytical pullout described in Section 3 as the mesh was refined.

Having detailed the scheme for modeling a stick–slip interface in a FE framework we now return to the crack bridging problem. The specimen shown in Fig. 11 is again bridged with a platelet of length $\frac{18}{11}a$, again at a distance of $\frac{5}{11}a$ behind the crack tip and the same mesh shown in Fig. 12 has been used. In this case the platelets are connected to the matrix via the stick–slip interface. The perfectly bonded case of $Q \approx 1.5$ showed large stress concentrations near the ends of the platelet; it is this case that will be examined now with the stick–slip interface.

For $Q \approx 1.5$ the slip zone and platelet slip will initiate from the embedded ends of the platelet. While the specific values of κ, $\tau_{\max}$, and τ_f do not significantly effect the shape of the stress distributions, they will determine under what loads the platelet interface will fail. For this example problem, which is used for qualitative analysis only, they were simply chosen in con-

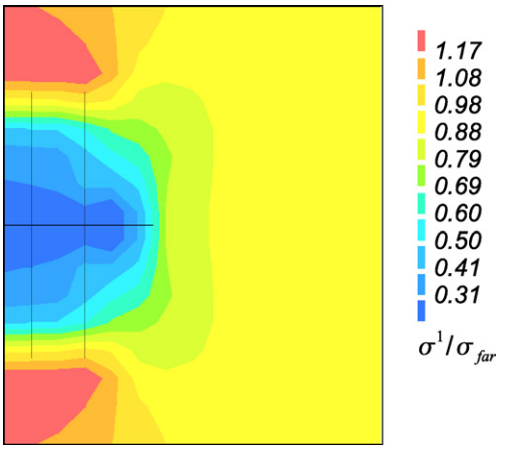

Fig. 14. Maximum principal stress distribution for two platelets bridging a crack tip with a perfectly bonded interface, $Q \approx 1.25$.

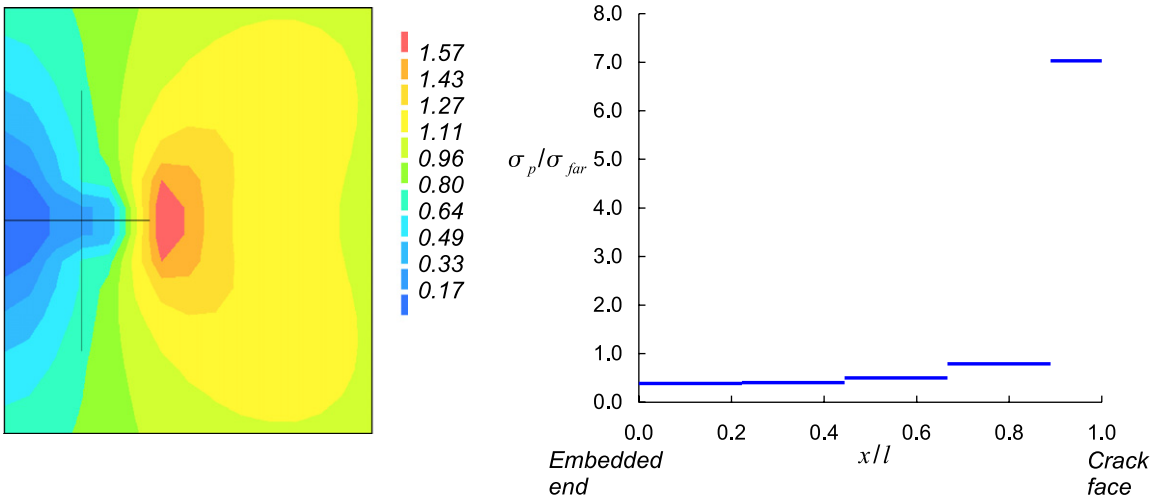

Fig. 15. Maximum principal stress distribution for platelet bridging a crack tip with a perfectly bonded interface, $Q \approx 26$ (left). Stress in each segment of one half of the platelet (right).

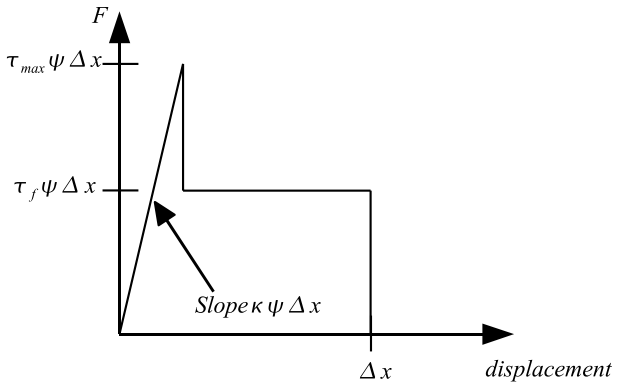

Fig. 16. Force-displacement relationship of nodal link on interior of platelet.

junction with the far field loading increments, to be able to observe the nature of crack bridging with a stick–slip interface. The load σ_{far} is incrementally increased. The SIF at the crack tip is measured at each loading and stress distributions are observed at several different loadings. These results will be discussed in the next section.

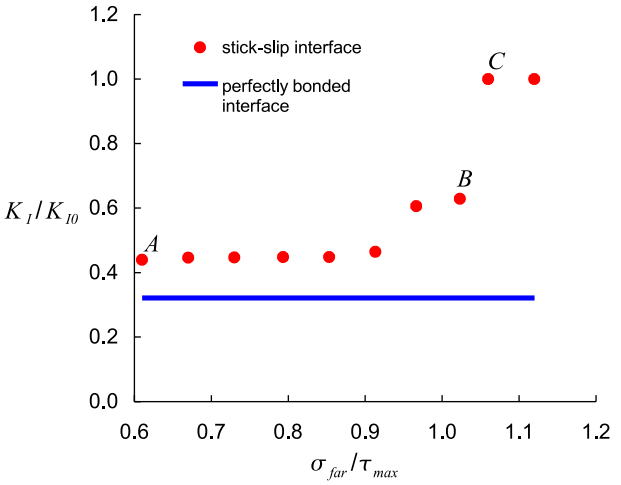

Fig. 17. Normalized Mode I bridged SIF as the far field tensile stress is increased for both the perfectly bonded and stick–slip bonded platelets, $Q \approx 1.5$.

5. SIF and Stress distributions for bridged crack

In Linear Elastic Fracture Mechanics (LEFM), under pure Mode I loading, the main driving force of crack growth is the SIF. In the geometry described in Fig. 11 the crack is loaded in mode I. A result of bridging the crack, with both perfectly bonded platelets and platelets with a stick–slip interface, the Mode I SIF, K_I, is reduced significantly. However, as the loading is increased for the stick–slip interface case, the platelet begins to slip and the SIF increases. Eventually, the platelet slips completely out of the matrix and the SIF is equal to that of an unbridged crack. Fig. 17 shows K_I of the bridged crack with two different interfaces as a fraction of, K_{I0}, as the far field load is incrementally increased for the case of $Q \approx 1.5$. The perfectly bonded bridging achieves a constant decrease in K_I. The stick–slip interface achieves a smaller decrease in K_I when the interface is fully stuck in the first load step. As the loading is increased, the embedded ends slip first followed by the rest and the platelet. K_I eventually reaches the unbridged value. Fig. 18 shows how the largest principal stress at the embedded ends of the platelet, σ^1, changes for both interfaces as the far field loading increases, for the case of $Q \approx 1.5$. It is seen that the in the perfectly bonded case these principal stress remains large while in the stick–slip case these stresses decrease as the platelet slips.

Figs. 13 and 14 indicate that the crack tip is well shielded from stress increase under the perfectly bonded bridging cases when $Q < 2$. It is likely that the crack will not grow, however new cracks may form at the highly stressed regions at the ends of the platelets. As Fig. 14 demonstrates, this problem may be exacerbated in situations where several platelet ends are near each other. This is the cause of plug pullout phenomenon; a phenomenon which essentially eliminates any advantages

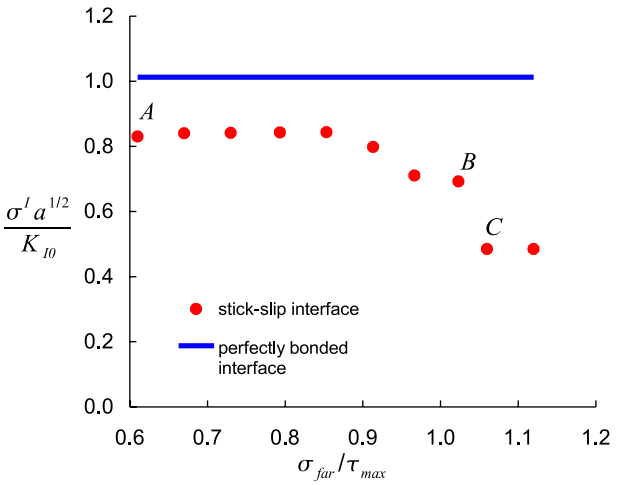

Fig. 18. Normalized largest principal stress at the embedded end of the platelet as the far field tensile stress is increased for both the perfectly bonded and stick–slip bonded platelets, $Q \approx 1.5$.

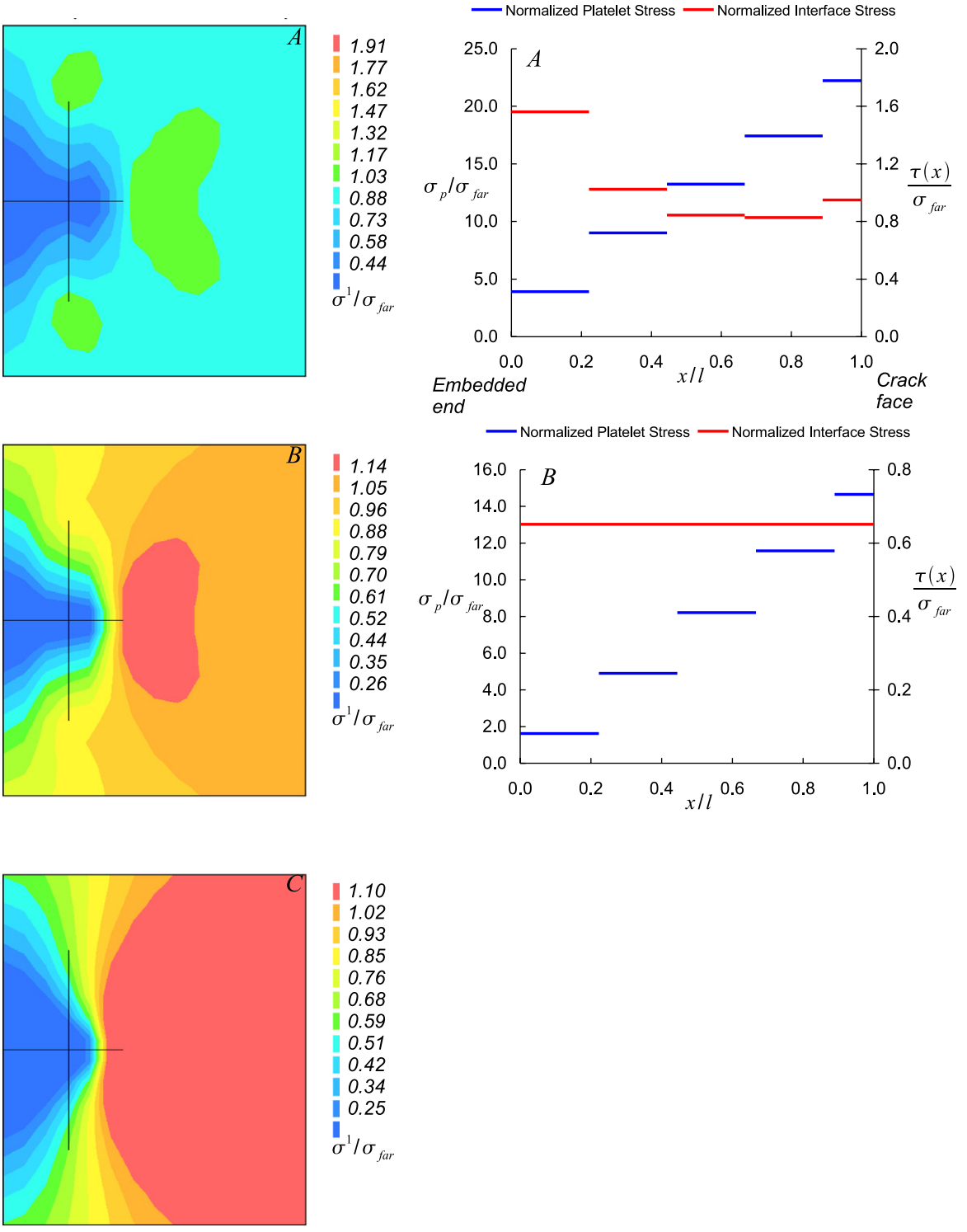

Fig. 19. Maximum principal stress contours for a crack bridged by a platelet with a stick–slip interface (left). Stresses in each segment of the platelet and the interface for one half of the platelet (right). Letters correspond to loading steps in Figs. 17 and 18. At load step C the stresses in the platelet and interface are zero.

gained by crack bridging. The evolution of the distribution of largest principal stress contours along with the stresses in each segment of one half of the platelet, σ_p, and stick–slip interface, $\tau(x)$, are shown in Fig. 19. The different distributions correspond to the loadings labeled with the letters A–C in Figs. 17 and 18. From these stress contour evolutions it can be seen that under small loads the crack tip is shielded well from stress. Also, there is a slight increase in stresses in the matrix near the

end of the platelets, but not nearly as much as in the perfectly bonded case. The crack tip always remains the location of the greatest stress concentration. As the load is increased the platelets slip eliminating stress increases near the ends of the platelets while shielding the crack tip less. Although no crack growth law was built into this numerical model, it is easy to predict that at some load K_I at the crack tip would become greater than the material could resist and the crack would grow from the crack tip. Consider a composite with discontinuous fibers randomly distributed throughout it; as the crack grows it would approach more fibers bridging it. The crack would repeatedly be shielded and then grow after each successive fiber slips.

6. Conclusions

In this paper, two types of interfaces for platelets bridging a crack were introduced, a perfectly bonded interface and a stick–slip interface. To validate the stick–slip interface a shear-lag model was developed. Both of these interfaces were modeled in FE and tested on a center crack in tension specimen in which the crack was bridged by two platelets. These FE and shear-lag models apply only for planar problems in which the ratio of the length to width of the platelets is very large and the crack is under Mode I loading only. For a case where Q was estimated to be less than two comparisons were made between the two types of interfaces for: K_I, σ^1, and the distributions of the largest principal stress. It was found that the perfectly bonded interface reduces K_I more but also introduces stress concentrations at the ends of the platelets.

The introduction of stress concentrations at the embedded ends of the platelets is undesirable since several platelets or fibers close together could initiate a new crack. This may lead to plug pullout phenomenon under higher loads. Plug pullout can be avoided by reducing the stress concentrations at the ends of the fibers. An imperfect interface between the fiber and the composite, such as the stick–slip interface discussed in this paper, can reduce these concentrations.

The stick–slip interface described in this paper is an idealized behavior of a real interface between a fiber and the matrix material which can be described by the three parameters κ, $\tau_{\max}$, τ_f. The stick–slip interface can be tailored to reduce K_I, though not as much as the perfectly bonded case, while making sure that any new stress concentrations at the platelet ends are small compared to the stress at the crack tip. The platelet slips before the stresses in the matrix at the platelet ends become significant.

In real composite systems the interfaces may behave differently than the two idealized interface types explored in this paper; however, the same interface design concepts will apply. Interfaces that are very strong compared to the matrix should be avoided in situations where stress concentrations form at the embedded ends, most likely composites with high concentrations of stiff fibers in a soft matrix. It is important to tailor the interface so that the fiber begins to slip before the stresses in the surrounding matrix become large enough to induce plug pullout. Once the fiber begins to slip the interface must provide enough resistance through the slip to slow down the crack growth and transfer stresses elsewhere in the material in order to achieve distributed deformation through microcracking.

Acknowledgements

This work is supported by the NASA University Research, Engineering and Technology Institute on Bio Inspired Materials (BIMat) under Award No. NCC-1-02037. This support is gratefully acknowledged. The authors would also like to thank Prof. Ilhan Aksay for his numerous helpful discussions.

Appendix I. (*in order of appearance*)

$S(x)$	local slip in interface
$\tau(x)$	local shear stress in interface
x	distance from embedded end of platelet
$\delta_p(x)$	displacement of platelet at point x
$\delta_m(x)$	displacement of matrix at point x
κ	bond modulus
$\tau_{\max}$	maximum shear stress of bonded interface
τ_f	frictional shear stress
A_m	cross-sectional area of matrix
w	width of pullout specimen
l	undeformed length of platelet
t	thickness of platelet
A_p	cross-sectional area of platelet
ψ	perimeter per unit length of platelet
P	applied load
Δ_l	free end displacement of platelet relative to matrix
$F(x)$	local force in platelet
Q, K, λ	dimensionless material parameters
E_p	Young's modulus of platelet

E_m Young's modulus of matrix
A_0, B_0, A_1, B_1, A_2, B_2 coefficients of force distribution functions
P_{crit} load at which slip zone is initiated
l_1 length of slip zone from free end of platelet
$F_b(x)$ force in stick zone of platelet
$F_{f_1}(x)$ force in slip zone at free end of platelet
S_{ab} change in slip accumulated along segment of interface from a to b
$\varepsilon_p(x)$ local strain in platelet
$\varepsilon_m(x)$ local strain in matrix
l_2 length of slip zone from embedded end of platelet
$F_{f_2}(x)$ force in slip zone at embedded end of platelet
l_3 length of stick zone of two way slip interface
l_d total length of slip zone of interface
Δ_0 total end slip of platelet accumulated at onset of dynamic full slip
u additional dynamic slip beyond Δ_0
a crack half length
σ_{far} far field loading on center crack in tension specimen
K_{I0} unbridged Mode I Stress Intensity Factor
σ_p stress in the platelet
Δx length of interface for one nodal link
K_I Mode I Stress Intensity Factor
σ^1 largest principal stress at embedded end of platelet

References

Belytschko, T., Black, T., 1999. Elastic crack growth in finite elements without remeshing. International Journal for Numerical Methods in Engineering 45, 601–620.

Bolander Jr., J.E., Saito, S., 1997. Discrete modeling of short-fiber reinforcement in cementitious composites. Advanced Cement Based Materials 6, 76–86.

Bolander Jr., J.E., Saito, S., 1998. Fracture analyses using spring networks with random geometry. Engineering Fracture Mechanics 61, 569–591.

Bolander, J.E., Sukumar, N., 2005. Irregular lattice model for quasistatic crack propagation. Physical Review B 71, 094106.

Carpinteri, A., Massabó, R., 1997. Continuous vs discontinuous bridged-crack model for fiber-reinforced materials in flexure. International Journal of Solids and Structures 34, 2321–2338.

Carpinteri, A., Spagnoli, A., Vantadori, S., 2006. An elastic–plastic crack bridging model for brittle-matrix fibrous composite beams under cyclic loading. International Journal of Solids and Structures 43, 4917–4936.

Kanda, T., Li, V.C., 1998. Interface property and apparent strength of high-strength hydrophilic fiber in cement matrix. Journal of Materials in Civil Engineering 10, 5–13.

Kanda, T., Li, V.C., 2006. Practical design criteria for saturated pseudo strain hardening behavior in ECC. Journal of Advanced Concrete Technology 4, 59–72.

Kullaa, J., 1998. Micromechanics of multiple cracking. Part I: fibre analysis. Journal of Materials Science 33, 4213–4224.

Leung, C.K.Y., Li, V.C., 1991. New strength-based model for the debonding of discontinuous fibres in an elastic matrix. Journal of Materials Science 26, 5996–6010.

Li, V.C., 1993. From micromechanics to structural engineering: the design of cementitious composites for civil engineering applications. Structural Engineering Japan Society of Civile Engineers 10, 37–48.

Li, V.C., 2003. On engineered cementitious composites (ECC): a review of the material and its applications. Journal of Advanced Concrete Technology 1, 215–230.

Li, V.C., Wu, H.C., 1992. Conditions for pseudo strain-hardening in fiber reinforced brittle matrix composites. Applied Mechanics Review 45, 390–398.

Marshall, D.B., Cox, B.N., 1988. A J-Integral method for calculating steady-state matrix cracking stresses in composites. Mechanics of Materials 7, 127–133.

Naaman, A.E., Namur, G.G., Alwan, J.M., Najm, H.S., 1991A. Fiber pullout and bond slip I: analytical study.. ASCE Journal of Structural Engineering 117, 2769–2790.

Naaman, A.E., Namur, G.G., Alwan, J.M., Najm, H.S., 1991B. Fiber pullout and bond slip. II: experimental validation.. ASCE Journal of Structural Engineering. 117, 2791–2800.

Prevost, J.H., Sukumar, N., 2003. Modeling quasi-static crack growth with the extended finite element method. Part I: computer implementation. International Journal of Solids and Structures 40, 7513–7537.

Redon, C., Li, V.C., Wu, C., Hoshiro, H., Saito, T., Ogawa, A., 2001. Measuring and modifying interface properties of PVA fibers in ECC matrix. Journal of Materials in Civil Engineering 13, 399–406.

Sheng, N., Boyce, M.C., Parks, D.M., Rutledge, G.C., Abes, J.I., Cohen, R.E., 2004. Multiscale micromechanical modeling of polymer/clay nanocomposites and the effective clay particle. Polymer 45, 487–506.

Tada, H., Paris, P.C., Irwin, G.R., 2000. The Stress Analysis of Cracks Handbook, third ed. ASME Press, New York.